Original Article

MOLECULAR METABOLISM

Hypothalamic expression of huntingtin causes distinct metabolic changes in Huntington's disease mice

Elna Dickson [1,*], Rana Soylu-Kucharz [1], Åsa Petersén [2], Maria Björkqvist [1]

ABSTRACT

Objective: In Huntington's disease (HD), the disease-causing huntingtin (HTT) protein is ubiquitously expressed and causes both central and peripheral pathology. In clinical HD, a higher body mass index has been associated with slower disease progression, indicating the role of metabolic changes in disease pathogenesis. Underlying mechanisms of metabolic changes in HD remain poorly understood, but recent studies suggest the involvement of hypothalamic dysfunction. The present study aimed to investigate whether modulation of hypothalamic HTT levels would affect metabolic phenotype and disease features in HD using mouse models.

Methods: We used the R6/2 and BACHD mouse models that express different lengths of mutant *HTT* to develop lean- and obese phenotypes, respectively. We utilized adeno-associated viral vectors to overexpress either mutant or wild-type HTT in the hypothalamus of R6/2, BACHD, and their wild-type littermates. The metabolic phenotype was assessed by body weight measurements over time and body composition analysis using dual-energy x-ray absorptiometry at the endpoint. R6/2 mice were further characterized using behavioral analyses, including rotarod, nesting-, and hindlimb clasping tests during early- and late-time points of disease progression. Finally, gene expression analysis was performed in R6/2 mice and wild-type littermates in order to assess transcriptional changes in the hypothalamus and adipose tissue.

Results: Hypothalamic overexpression of mutant HTT induced significant gender-affected body weight gain in all models, including wild-type mice. In R6/2 females, early weight gain shifted to weight loss during the corresponding late stage of disease despite increased fat accumulation. Body weight changes were accompanied by behavioral alterations. During the period of early weight gain, R6/2 mice displayed a comparable locomotor capacity to wild-type mice. When assessing behavior just prior to weight loss onset in R6/2 mice, decreased locomotor performance was observed in R6/2 females with hypothalamic overexpression of mutant HTT. Transcriptional downregulation of beta-3 adrenergic receptor (B3AR), adipose triglyceride lipase (ATGL), and peroxisome proliferator-activated receptor-gamma (PPARγ) in gonadal white adipose tissue was accompanied by distinct alterations in hypothalamic gene expression profiles in R6/2 females after mutant HTT overexpression. No significant effect on metabolic phenotype in R6/2 was seen in response to wild-type HTT overexpression.

Conclusions: Taken together, our findings provide further support for the role of HTT in metabolic control via hypothalamic neurocircuits. Understanding the specific central neurocircuits and their peripheral link underlying metabolic imbalance in HD may open up avenues for novel therapeutic interventions.

© 2022 The Authors. Published by Elsevier GmbH. This is an open access article under the CC BY-NC-ND license (http://creativecommons.org/licenses/by-nc-nd/4.0/).

Keywords Huntington's disease; Metabolic alterations; Hypothalamus; Adipose tissue

1. INTRODUCTION

Huntington's disease (HD) is caused by a pathological expansion of CAG repeats in exon 1 of huntingtin (*HTT*), leading to the production of mutant HTT (mHTT) protein associated with widespread neuropathology [1,2]. HD is characterized by choreic movements, psychiatric symptoms, and cognitive decline, but is accompanied by metabolic alterations. Clinical findings of an HD metabolic profile include elevated energy expenditure [3], progressive weight loss [4,5], as well as impaired cholesterol- and fatty acid synthesis [6,7]. Endocrine alterations have also been described [8—10]. Based on longitudinal data from Enroll-HD, a worldwide observational study of HD families, van

[1]Brain Disease Biomarker Unit, Wallenberg Neuroscience Center, Department of Experimental Medical Science, Lund University, BMC A10, 221 84 Lund, Sweden [2]Translational Neuroendocrine Research Unit, Department of Experimental Medical Science, Lund University, BMC D11, 221 84 Lund, Sweden

*Corresponding author. Wallenberg Neuroscience Center, Department of Experimental Medical Science, BMC A10, Lund University, 22184 Lund, Sweden. E-mail: elna.dickson@med.lu.se (E. Dickson).

Abbreviations: 36B4, acidic ribosomal phosphoprotein P0; AAV, adeno-associated viral vector; ATGL, adipose triglyceride lipase; AUC, the area under curve; B3AR, beta-3 adrenergic receptor; BAC, bacterial artificial chromosome; BAT, brown adipose tissue; BMI, body mass index; BDNF, brain-derived neurotrophic factor; DAB, 3,3′-diaminobenzidine; DEXA, dual-energy x-ray absorptiometry; DRD2, dopamine receptor D2; GFP, green fluorescent protein; HD, Huntington's disease; HPRT, hypoxanthine-guanine phosphoribosyltransferase; HTT, huntingtin; PFA, paraformaldehyde; PPARγ, peroxisome proliferator-activated receptor-gamma; POMC, pro-opiomelanocortin; RER, respiratory exchange ratio; RPL13a, ribosomal protein L13a; Syn-1, synapsin-1 promoter; UCP1, uncoupling protein 1; WAT, white adipose tissue; WT, wild-type

Received December 21, 2021 • Accepted January 5, 2022 • Available online 7 January 2022

https://doi.org/10.1016/j.molmet.2022.101439

 © 2022 The Authors. Published by Elsevier GmbH. This is an open access article under the CC BY-NC-ND license (http://creativecommons.org/licenses/by-nc-nd/4.0/).

der Burg and co-workers demonstrated that body mass index (BMI) is significantly associated with disease progression, where patients with a high BMI at baseline presented slower rates of motor, functional and cognitive decline independent of their CAG repeat number [11]. Metabolic defects such as weight loss may result from mHTT-mediated neuropathology of vital energy-regulating structures in the brain but could also arise from direct effects of mHTT expression in peripheral tissues [12,13].

Hypothalamus serves as the central communication between the brain and periphery, integrating systemic signals to maintain body homeostasis, regulating essential physiological functions such as sleep, endocrine function, food intake, and energy balance [14]. Neuropathological changes in the hypothalamus as well as non-motor symptoms occur early in HD patients and often precede clinical diagnosis [15,16]. Therefore, several studies have been conducted to investigate the pathological role of mHTT in the hypothalamus and its subsequent impact on HD phenotype.

Thus far, it has been shown that common pathological features of HD models can be reproduced in wild-type (WT) mice by targeted overexpression of mHTT exclusively in hypothalamic neurons [17,18]. Selective deletion of mHTT in the hypothalamus has been shown to be sufficient in order to ameliorate hyperphagic obesity and depressive-like phenotype in the full-length bacterial artificial chromosome (BAC)-mediated transgenic HD mouse model (BACHD) [17,19]. Furthermore, significant hypothalamic pathology occurs in the R6/2 model [20—22]. R6/2 mice express exon 1 of the human HD gene with varying CAG repeats [23] and develop progressive motor, psychiatric- and metabolic impairments, mimicking clinical HD [3,21,24].

Several studies also suggest the role of wild-type HTT (wtHTT) in the control of whole-body energy metabolism. WtHTT is ubiquitously expressed throughout the body and partakes in several vital physiological processes [25] many of which are altered in HD. Through the ubiquitous expression of full-length human mHTT, BACHD mice become progressively obese with leptin- and insulin resistance [17], and YAC18 mice expressing a full-length human wtHTT fragment display dose-dependent increases in body weight and increased body composition [26].

Given that HTT is ubiquitously expressed in the body and hypothalamus-specific expression of HTT in WT mice is enough to recapitulate HD neuropathology and metabolic dysfunction, our aim in this study was to investigate the effects of wtHTT and mHTT hypothalamic overexpression in HD mouse models. In line with previous studies where female mice demonstrate the largest effect on body weight change [27], we chose to focus on assessing metabolic parameters in female experimental groups. We hypothesized that increased levels of HTT in the hypothalamus could modify the severity of HD pathology. To address this idea, we used adeno-associated viral (AAV) vectors to selectively overexpress wtHTT and mHTT in hypothalamic neurons of the BACHD, R6/2 mice, and their WT littermates.

2. MATERIALS AND METHODS

2.1. Ethical considerations

The experimental procedures were performed in accordance with guidelines stated in the ethical permits approved by the Animal Ethics Committee Malmö/Lund Animal Welfare and Ethics Committee in Lund-Malmö, Sweden.

2.2. Viral vector injections

AAV of serotype rAAV2/5 expressing N-terminal fragments of human HTT with 853 amino acids in length under the control of the human Synapsin-1 (Syn-1) promoter was used [17]. Exon 1 of the HTT transgenes had a CAG repeat length that corresponded to either wtHTT (18 CAG repeats; HTT853-18Q) or mHTT (79 CAG repeats; HTT853-79Q). In the BACHD study, a rAAV5-green fluorescent protein (GFP) vector was used as a control group to assess transgene efficiency. Mice were injected bilaterally in the hypothalamus at 8 weeks of age with 0.5 μl/hemisphere using stereotaxic surgery as previously described [18]. Vector concentrations were the following: rAAV5-HTT853-79Q; 1.6—2.14 Ex14 genome copies (GC)/ml; rAAV5-HTT853-18Q; 1.4—2.1 Ex14 GC/ml and rAAV5-GFP; 5.7 Ex13 GC/ml. Correct targeting of the hypothalamus and sufficient transgene expression were validated by histology (sc-8767; Santa-Cruz Biotechnology, US) or qRT-PCR for HTT (Table S1).

2.3. Animals

All mice used in the study were group-housed (2—5/cage) under standard conditions (12 h light/dark cycle, 22 °C) in environmentally enriched universal Innocage mouse cages (InnoVive, San Diego, CA, US) with *ad libitum* access to water and normal chow diet (25kGy; Special Diets Services, UK).

BACHD mice were of the FVB/N strain and expressed full-length mutant HTT with 97 CAG repeats [28]. BACHD and WT littermates were sacrificed at 29 weeks post-injection (approximately 9 months of age).

The transgenic R6/2 mouse model, first developed in 1996 [23], displays a rapid and reproducible progression of HD-like symptoms, such as motor dysfunction, weight loss, and striatal volume reduction [23,29]. The R6/2 mice used in the current study had a CAG repeat size range between 258 and 340, resulting in a slower disease progression compared to R6/2 mice with 150 CAGs [30]. In line with this, we have previously shown that R6/2 mice with 273—285 CAG display increased neurofilament light protein levels in cerebrospinal fluid accompanied by reduced body weight and brain atrophy at 18 weeks of age [31]. In the present study, R6/2 and WT littermates were sacrificed at 11 weeks post-injection (19 weeks of age), corresponding to the mid/late-stage of disease [30,31]. The R6/2 mice were bred on a CBAxC57BL/6J background through crossing heterozygous R6/2 males with WT females. CAG repeat lengths of the colony were determined from ear biopsies by Laragen (Laragen Inc, US).

2.4. Metabolic assessments

2.4.1. Body weight and DEXA analysis

For R6/2 mice and their WT littermates, body weights were recorded weekly starting from surgery week (8 weeks of age) until sacrifice at 11 weeks post-injection (19 weeks of age). At sacrifice, dual-energy x-ray absorptiometry (DEXA; Lucar PIXImus2, Lunar Corporation, US) was performed and frozen adipose tissue was collected and snap-frozen for qRT-PCR analysis.

Body weights were recorded for BACHD mice and their WT littermates starting at 4 weeks post-injection and then once during weeks 6, 10-, 14-, 16-, 20-, 22-, 24- and 26 post-injection. DEXA analysis was carried out at 29 weeks post-injection.

2.4.2. Food intake measurements

Food intake measurements were performed according to a grouped setup to enable progressive monitoring of food intake in a natural enriched home cage environment and to avoid potential stressors associated with individual housing. After surgery, R6/2 females and their WT littermates were divided into environmentally enriched universal Innocage mouse home cages (InnoVive, US) based on genotype

 © 2022 The Authors. Published by Elsevier GmbH. This is an open access article under the CC BY-NC-ND license (http://creativecommons.org/licenses/by-nc-nd/4.0/).

(WT or R6/2) and vector (uninjected, 18Q or 79Q) with 2–4 mice/cage and kept under the standard housing conditions as described above. An electronic scale was used to weigh and compare remaining food in grams on days 0, 3, and 7 of each week. Total weekly food intake for each cage is expressed as g/mouse/day. Using this set-up, each experimental group was represented by one cage. For WT uninjected mice we had to make an exception as one mouse had to be excluded during the experiment.

2.4.3. Indirect gas calorimetry

Indirect gas calorimetry was performed using the PhenoMaster Automatic Home Cage Phenotyping system (TSE Systems, Germany). Female mice with matching vector injection (WT or R6/2) and genotype (uninjected, 18Q or 79Q) were analyzed in groups of $n = 2–3$. Prior to data measurements, mice were first habituated for 24 h to the PhenoMaster water bottles inside their respective home cages and then transferred for a 24-h acclimatization step in fully equipped PhenoMaster cages. Bedding material from the home cage was provided as enrichment to reduce stress. Metabolic parameters were recorded during 24 h, with a sample interval of 3 min/cage. Metabolic parameters (oxygen consumption; VO_2 and respiratory exchange ratio; RER) were calculated using a correction for the total body weight in the cage and presented as the mean for each cage in the light phase, dark phase, and over 24 h.

2.5. Behavioral analyses

Behavioral tests were performed at 4- and 8 weeks post-injection in WT and R6/2 mice. Prior to all behavioral tests, mice were habituated for 1 h. With an exception for the nest-building test (2.5.1.), all tests were performed during the light phase period.

2.5.1. Nest-building

One hour prior to the dark phase, mice were individually housed in cages with enrichment materials removed and with *ad libitum* access to food and water. Nesting material was placed at the center of the cage and mice were left overnight. In the morning, mice were returned to their home cages and used nesting material was weighed on an electronic scale. Nesting scores were assigned according to the 1 to 5 point scoring protocol suggested by Deacon et al. [32] where percentage material used and nest structure is taken into account.

2.5.2. Open field

To assess general locomotor activity, mice were individually placed in the center of a 40 × 40 cm arena enclosed by transparent Plexiglas walls. Activity in the arena was recorded for 60 min with data collected every 5 min using the Any-Maze Video tracking software (Stoelting Co, Ireland). Each station was cleaned with 30% ethanol between each test. The total distance moved during 60 min was used to evaluate locomotor performance in each animal.

2.5.3. Rotarod

Motor coordination and balance were assessed with a rotarod test using the Rotamex 4/8 system (Rota Rod Columbus Instruments, US). The mice were first trained for one round on the rotarod at a fixed speed of 4 rpm for 5 min followed by a 1 h rest prior to the test phase. The test phase consisted of three accelerating tests (4–40 rpm over 5 min) separated by a 15 min rest between each test. Mean latency to fall in the three tests was used as a measure of rotarod performance. The rotarod apparatus was cleaned with 30% ethanol between each test.

2.5.4. Hindlimb clasping

Hindlimb-clasping phenotypes have been described in the R6/1 and R6/2 models [22]. When suspended by the tail towards a horizontal surface, healthy adult rodents splay all four limbs outwards, away from the abdomen [33]. Mice were carefully lifted by the base of the tail from a horizontal surface at a distance just within reach for the forelimbs and were suspended for 15 s while recorded with a video camera. One trial was performed for each time point. Scores were assigned from 0 to 3 according to criteria adopted by Guyenet et al. [34], where a score of 3 represented the most severe phenotype.

2.6. Immunohistochemistry

Brains for histological analysis were fixed in 4% paraformaldehyde (PFA) by transcardial perfusion. Mice under terminal sodium pentobarbital anesthesia (Apoteksbolaget, Lund, Sweden) were perfused with room-tempered saline (0.9%) followed by cold 4% PFA for 10 min. Brains were dissected and placed in 4% PFA at 4 °C for 24 h and then switched to 25% sucrose at 4 °C for 24–48 h. Brains were cut in a series of 30 μm coronal sections and stored at −20 °C in an antifreeze solution (30% glycerol, 30% ethylene glycol solution in PBS). Free-floating brain sections were rinsed 3 times with 0.05 M Tris-buffered saline (TBS) followed by a quenching reaction (10% MeOH, 3% H_2O_2 in TBS) for 30 min at room temperature (RT). After rinsing 2 times in TBS followed by 1 time in TBS-T, sections were pre-incubated for 1 h at RT with blocking solution (5% normal horse serum in 0.25% Triton-X in TBS). The sections were then incubated overnight with primary anti-HTT antibody (sc-8767; Santa-Cruz Biotechnology, US) prepared in a 1% bovine serum albumin (BSA)/TBS-T solution. Following completion of primary antibody treatment, sections were rinsed 3 times in TBS-T and then incubated with secondary horse anti-goat antibody (BA9500; Vector Laboratories, US) prepared in 1% BSA/TBS-T for 1 h at RT. Sections were rinsed 3 times with TBS-T and incubated with avidin-biotin-peroxidase complex solution (PK-6100, Vector Laboratories, US) in TBS for 1 h. Three final washing steps, 2 times in TBS-T followed by 1 time in TBS were performed prior to visualization with 3, 3′-diaminobenzidine (DAB). Stained sections were mounted on gelatin-coated glass slides, dried overnight at RT, dehydrated through ascending alcohol concentrations, and cleared in xylene, before cover-slipping with DPX mounting medium (Sigma–Aldrich, US).

2.7. Gene expression analyses

Hypothalamic tissue, gonadal white adipose tissue (WAT), and brown adipose tissue (BAT) were dissected on ice and were snap-frozen in liquid nitrogen for storage at −80 °C. RNA was isolated using the RNeasy Lipid Tissue Mini Kit (Qiagen, US) for the hypothalamus and the E.Z.N.A. Total RNA Kit II (Omega Bio-Tek, US) for adipose tissue. Reverse transcription was carried out using 1 μg of sample RNA with the Superscript IV Reverse Transcriptase kit (Invitrogen, US) according to the manufacturer's protocol. SYBR Green I Master (Roche, Switzerland) based qRT-PCR was performed using LightCycler 480 (Roche, Switzerland) using a three-step amplification protocol. Calculations of relative gene expression were performed using the 2-ΔΔCT method [35] and the relative expression was normalized to the glyceraldehyde 3-phosphate dehydrogenase (GAPDH) and β-actin housekeeping genes in hypothalamus, β-actin and ribosomal protein L13a (RPL13a) in BAT and acidic ribosomal phosphoprotein P0 (36B4) and hypoxanthine-guanine phosphoribosyltransferase (HPRT) in gonadal WAT. Primer sequences are shown in Table S1.

 © 2022 The Authors. Published by Elsevier GmbH. This is an open access article under the CC BY-NC-ND license (http://creativecommons.org/licenses/by-nc-nd/4.0/).

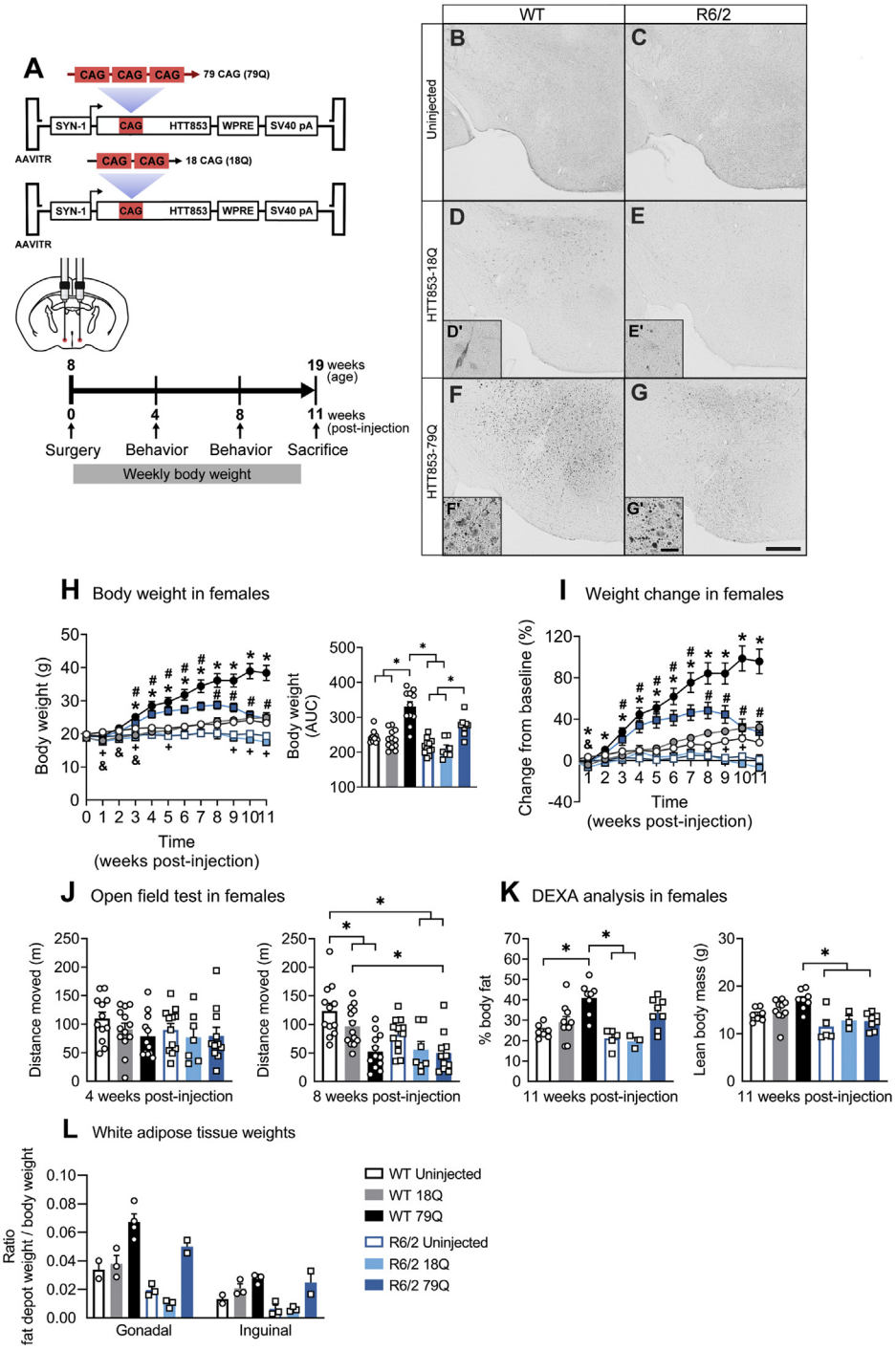

Figure 1: Increased body weight in the R6/2 mouse model of HD after overexpression of 18Q or 79Q HTT fragments in the hypothalamus. (A) Experimental overview. Eight-week old WT and R6/2 mice were bilaterally injected in the hypothalamus with AAV vectors overexpressing an HTT transgene consisting of the first 853 amino acids with a CAG repeat length of either 18 CAG (18Q; wild-type HTT) or 79 CAG (79Q; mutant HTT). HTT transgene expression was driven by the Syn-1 promoter to specifically target hypothalamic neurons. (B–G) Histological images from the endpoint of 11-weeks post-injection show diffuse HTT inclusion formation in the hypothalamus of WT 79Q and R6/2 79Q mice after AAV injections. (B) WT uninjected, (C) R6/2 uninjected, (D) WT 18Q, (E) R6/2 18Q, (F) WT 79Q, and (G) R6/2 79Q. Scale bar in (G) 200 μm and applies to (B)–(G); in (G′) 20 μm and applies to (D′-G′). (H–I) Time-course of body weight progression in female mice, analyzed using a linear mixed model followed by pairwise comparisons using differences of least squares means (genotype*vector*time). *$p < 0.05$ WT 79Q vs WT uninjected, &$p < 0.05$ WT 18Q vs WT uninjected, +$p < 0.05$ R6/2 uninjected vs WT uninjected and #$p < 0.05$ R6/2 79Q vs R6/2 uninjected at each timepoint. For the full list of group comparisons, see Supplemental Statistical Results. (H) For female groups, 79Q expression in the hypothalamus induced distinct weight progressions in both WT and R6/2 mice ($n = 7–12$/group). AUC to estimate the overall change in body weight showed a significant increase in both WT 79Q and R6/2 79Q compared to the respective uninjected groups ($n = 7–12$/group; Kruskal–Wallis test followed by Dunn's *post hoc*). (I) Weight change from baseline was affected in both WT and R6/2 with 18Q or 79Q overexpression ($n = 7–12$/group). (J) Open field test in females at 4 weeks post-injection showed no difference in distance moved, while significantly lower distance moved was observed in all 18Q and 79Q groups compared to WT uninjected at 8 weeks post-injection ($n = 7–13$/group; 2-way ANOVA followed by Tukey's *post hoc*). (K) DEXA analyses of % body fat and lean mass in female mice show increased body fat without changes in lean mass in WT 79Q ($n = 3–10$/group). (L) Gonadal and inguinal white adipose tissue weights in females, presented by the ratio of fat depot weight to body weight ($n = 2–4$/group) (Supplemental Statistical Results). Data are presented as mean ± SEM. **Abbreviations:** WT = wild-type, 18Q = HTT853-18Q vector, 79Q = HTT853-79Q vector.

 © 2022 The Authors. Published by Elsevier GmbH. This is an open access article under the CC BY-NC-ND license (http://creativecommons.org/licenses/by-nc-nd/4.0/).

2.8. Statistical analysis

Data were assessed for normal distribution using the Kolmogorov–Smirnov test. For time-course body weight datasets that fulfilled the criteria for parametric distribution, a linear mixed model was employed and performed using Proc Mixed in SAS (SAS Enterprise Guide 6.1 for Windows, SAS Institute Inc., US). Body weight (or body weight change) was put as dependent variables and the fixed effects in the model were vector, genotype, time, vector*genotype, vector*time, genotype*time, and vector*genotype*time. The repeated covariance type chosen was unstructured. The full list of comparisons can be found in Supplemental Statistical Results. All other statistical analyses were performed using GraphPad Prism 9 (GraphPad Software Inc., US). Parametric data were analyzed using 2-way ANOVAs to estimate the main effects of vector and genotype and interaction effects of vector*genotype followed by Tukey's multiple comparison *post hoc* test. Data that did not pass the normality test were analyzed with the Kruskal–Wallis test followed by Dunn's *post hoc* test. Statistical significance was considered at $p < 0.05$. Nonparametric data with low sample numbers (Figures 1L and 2, Suppl. Figure S1, S2, S3) are presented using descriptive statistics (Supplemental Statistical Results). Data are presented as mean ± SEM.

3. RESULTS

3.1. Overexpression of mutant HTT in hypothalamus causes progressive changes in body weight and body composition in R6/2 and BACHD mice

HTT inclusion bodies are a pathological hallmark of clinical HD [36,37] and R6/2 mice [38,39], and inclusion formation can be induced in the hypothalamus of WT mice by viral vector-mediated overexpression of mHTT fragments [17]. We, therefore, assessed brain sections by histology after bilateral injections of AAV vectors expressing HTT fragments of 18Q repeats (HTT853-18Q; wtHTT, hereafter referred to as 18Q) and 79Q repeats (HTT853-79Q; mHTT, hereafter referred to as 79Q) at the 11-weeks post-injection endpoint (Figure 1A). Both WT and R6/2 expressing 18Q displayed diffuse HTT cytoplasmic staining, while 79Q overexpression resulted in widespread HTT inclusion formation (Figure 1B–G).

Hypothalamic HTT overexpression in female mice caused pronounced weight changes. Both WT 79Q and R6/2 79Q females displayed rapid early weight gain compared to uninjected groups with significant increases in area under the curve (AUC) for the same dataset compared to their respective uninjected groups (Figure 1H). Peak body weight for

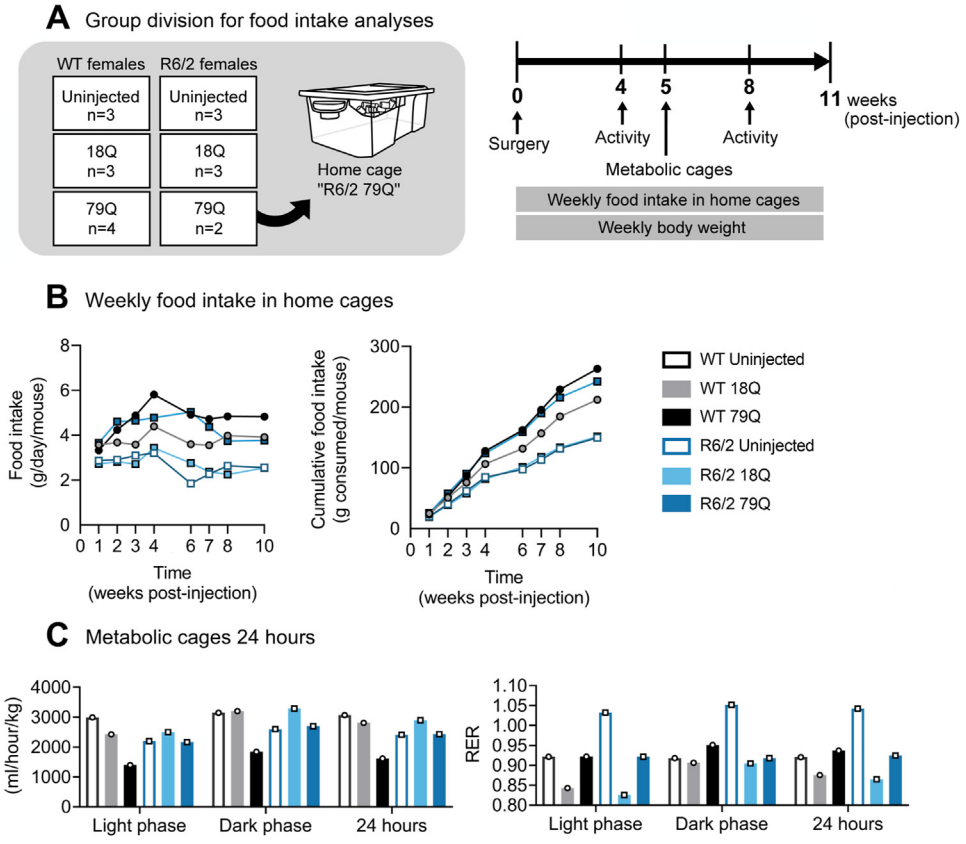

Figure 2: Evaluation of food intake and metabolic rate in 18Q and 79Q females using a grouped cage setup. (A) Experimental overview. For assessment of weekly food intake, females of the same genotype (WT or R6/2) and HTT vector injection (18Q, 79Q, or uninjected) were divided into groups of n = 2–4 in home cages for analyses from surgery week (time point 0) to endpoint (11 weeks post-injection). (B) Weekly food intake in home cages expressed as g/mouse/day and cumulative consumption (g/mouse/week) for each cage from 1 to 10 weeks post-injection. No food intake measurements were taken at 5 and 9 weeks post-injection due to metabolic cage trials. For R6/2 79Q, n = 3 at 1–4 weeks post-injection followed by n = 2 at 6–10 weeks post-injection. Data is presented as mean ± SEM (n = 2–4/group). Descriptive statistics are available (Supplemental Statistical Results). (C) At 5 weeks post-injection, mice from each experimental group were analyzed in groups in the metabolic cages over 24 h. Number of mice housed in each metabolic cage shown in C: WT uninjected: n = 3, WT 18Q: n = 3, WT 79Q: n = 2, R6/2 uninjected: n = 3, R6/2 18Q: n = 3, R6/2 79Q: n = 2. For measurements of VO_2 and subsequent calculation of RER, a correction for total body weight in each cage was used (ml/hour/kg) and presented as the mean for each cage in the light phase, dark phase, and over 24 h. **Abbreviations:** 18Q = HTT853-18Q vector, 79Q = HTT853-79Q vector, VO_2= oxygen consumption, RER = respiratory exchange ratio.

 © 2022 The Authors. Published by Elsevier GmbH. This is an open access article under the CC BY-NC-ND license (http://creativecommons.org/licenses/by-nc-nd/4.0/).

WT 79Q was recorded at 10 weeks post-injection, in contrast to R6/2 79Q at 8 weeks post-injection, notably before the onset of weight loss (WT 79Q: 38.91 g, R6/2 79Q: 28.72 g). While R6/2 79Q females showed significant weight changes, no overall impact on body weight was seen for the R6/2 18Q and R6/2 uninjected groups (Figure 1I). At 9–11 weeks post-injection, R6/2 female uninjected mice displayed significantly lower body weights compared to WT uninjected, indicative of weight loss onset. Despite the similar pattern of reduced weight in R6/2 79Q to R6/2 uninjected from 9 weeks post-injection (R6/2 79Q: 10 vs. 9 weeks: −2.34 g; 11 vs. 10 weeks: −0.94 g), endpoint body weight was significantly higher. To assess whether weight phenotypes were caused by altered locomotor activity, an open field test was performed at 4 weeks post-injection during early weight gain and at 8 weeks post-injection just prior to weight loss in R6/2 mice. Early weight changes in females were not associated with reduced locomotor activity as assessed at 4 weeks post-injection (Figure 1J). At 8 weeks post-injection, activity was reduced in WT 18Q, WT 79Q, R6/2 18Q, and R6/2 79Q females compared to WT uninjected. 2-way ANOVA of 8 weeks post-injection open field data showed a significant main effect of vector ($p < 0.0001$) and genotype ($p = 0.0024$). Body composition analyzed using DEXA at endpoint showed a significant increase in percentage body fat in WT 79Q mice compared to WT uninjected (Figure 1K), while no changes in lean mass were observed. In a smaller group of female mice ($n = 2–4$/group), gonadal visceral WAT depots and inguinal subcutaneous WAT depots were weighed at sacrifice (WT 79Q: 3.04 ± 0.36 g gonadal WAT vs. WT uninjected: 0.81 ± 0.14 g; R6/2 79Q: 1.49 ± 0.15 g gonadal WAT vs. R6/2 uninjected: 0.38 ± 0.07 g). The ratio of fat depot weight to body weight is shown in Figure 1L and descriptive statistics are available for both datasets (Supplemental Statistical Results).

We performed the same experimental setup in a smaller group of R6/2 males and their WT littermates. Despite the expression of mHTT and wtHTT in the hypothalamus, R6/2 79Q male mice ($n = 2$) also had a weight loss phenotype similar to female mice (Figure S1). Data are presented using descriptive statistics (Supplemental Statistical Results). Notably, a few injected males were sacrificed earlier at 10 weeks post-injection due to severe motor deficits and weight loss. Symbols have been adjusted in affected datasets (Figure S1).

Lastly, we investigated the effects of 18Q and 79Q HTT overexpression in the hypothalamus in the full-length BACHD model. In contrast to R6/2 mice characterized by a lean phenotype, BACHD mice express full-length HTT with a shorter CAG repeat (97Q) and develop hyperphagic obesity and have a slower disease progression [28]. Data are presented using descriptive statistics (Supplemental Statistical Results). Hypothalamic overexpression of 18Q induced HTT cytoplasmic immunoreactivity in BACHD and WT littermates while diffuse HTT inclusion formation was observed in the 79Q groups (Figures S2A–F). Similarly, to what we observed in the R6/2 model, WT and BACHD mice injected with the 79Q overexpression vector in the hypothalamus gained weight (AUC WT 79Q: 1030.76 vs. WT uninjected: 599.99 and BACHD 79Q: 1253.28 vs. BACHD uninjected: 996.02) (Figure S2G). In addition, a similar but less pronounced effect was seen for 18Q overexpression (AUC WT 18Q: 954.38, BACHD 18Q: 1087.87). Weight changes in WT mice were accompanied by increases in percentage body fat assessed using DEXA (WT 18Q: +13.16% body fat and WT 79Q: +11.83% vs. WT uninjected) (Figure S2H). A reduced effect on body weight and body composition was seen in a smaller group of WT and BACHD (Figures S2I, S2J) (Supplemental Statistical Results). GFP vectors used as a control group to assess transgene efficiency did not consequently change in metabolic parameters from hypothalamic overexpression.

3.2. Altered food intake and metabolic rate caused by hypothalamic 79Q overexpression

We next assessed food intake and metabolic rate as possible contributing factors to the pronounced body weight phenotype observed in WT 79Q and R6/2 79Q females. To avoid stress from individual caging affecting metabolic parameters [40], we used a grouped cage set up to assess food intake ($n = 2–4$ mice per cage, one cage per genotype and vector to represent each group with exception for a cage representative of WT uninjected females (section 2.4.2.) (Figure 2A). For R6/2 79Q food intake, 3 were housed in a cage at 0–4 weeks post-injection followed by 2 at 6–10 weeks post-injection. Food intake recordings were excluded at 5- and 9 weeks post-injection due to metabolic cage trials. At 1–4 weeks post-injection WT 79Q and R6/2 79Q increased their weekly food intake (WT 79Q: +2.48 g/mouse/day, R6/2 79Q: +1.12 g/mouse/day) (Figure 2B). Cumulative food intake from available recordings from 1 to 10 weeks post-injection showed the highest progressive consumption in WT 79Q and R6/2 79Q groups. Lastly, we used an automated metabolic cage system to assess metabolic rate during the period of 79Q weight gain at 5 weeks post-injection. Previous studies utilizing metabolic cages have indicated that this novel environment could affect mouse welfare [40,41] and due to inadequate acclimatization we avoided individually housed mice. We therefore carefully considered strategies to perform metabolic cage housing as stress-free as possible and used a grouped setup ($n = 2–3$ mice per cage, one cage per genotype and vector to represent each experimental group). For WTs, the following VO_2 over 24 h was recorded for each cage (n = number of housed mice in a cage): WT uninjected ($n = 3$ mice): 3068.96 ml/h/kg, WT 18Q ($n = 3$): 2810.22 ml/h/kg and WT 79Q ($n = 2$): 1615.11 ml/h/kg (Figure 2C). For R6/2: R6/2 uninjected ($n = 3$): 2410.48 ml/h/kg, 18Q ($n = 3$): 2895.43 ml/h/kg and 79Q ($n = 2$): 2427.91 ml/h/kg (Figure 2C).

3.3. Hypothalamic 79Q HTT overexpression causes behavioral alterations

Next, we characterized the behavioral phenotype of WT and R6/2 mice with hypothalamic overexpression of 18Q and 79Q HTT. Behavioral phenotypes were assessed at 4 weeks post-injection corresponding to the period of early weight gain and at 8 weeks post-injection in female mice. The 8-week timepoint corresponds to prior to the onset of weight loss in R6/2 79Q. Male mice data are presented in Figure S3.

Rotarod test was used to assess motor phenotype. At 4 weeks post-injection, no significant change was found for WT 79Q and R6/2 79Q females when compared to their respective uninjected groups (Figure 3A). Trends towards shorter latency to fall were seen in WT 18Q ($p = 0.0540$) and R6/2 18Q ($p = 0.0641$) compared to WT uninjected. At 8 weeks post-injection, R6/2 79Q females had a significantly lower latency to fall compared to WT uninjected.

The nesting test can be used as a general assessment of well-being and is sensitive to brain lesions and genetic mutations [32,42,43]. A deficiency in nest-building behavior has previously been described in our R6/2 cohort [44]. Here, we similarly observed low nest-building scores for R6/2 female and male groups compared to WT uninjected at 4- and 8 weeks post-injection with no significant change in this phenotype in response to 18Q and 79Q injections (Figure 3B, Figure S3B).

Hindlimb clasping phenotypes are present in various mouse models of neurodegeneration [34] and have previously been described in R6/2 mice [23]. At 8 weeks post-injection, just prior to weight loss, a few R6/2 mice started displaying clasping behaviors (Figure 3C, Figure S3C). All R6/2 79Q males analyzed at this time point displayed clasping behaviors ($n = 5$, mean score 2.5 ± 0.32) (Figure S3C).

 © 2022 The Authors. Published by Elsevier GmbH. This is an open access article under the CC BY-NC-ND license (http://creativecommons.org/licenses/by-nc-nd/4.0/).

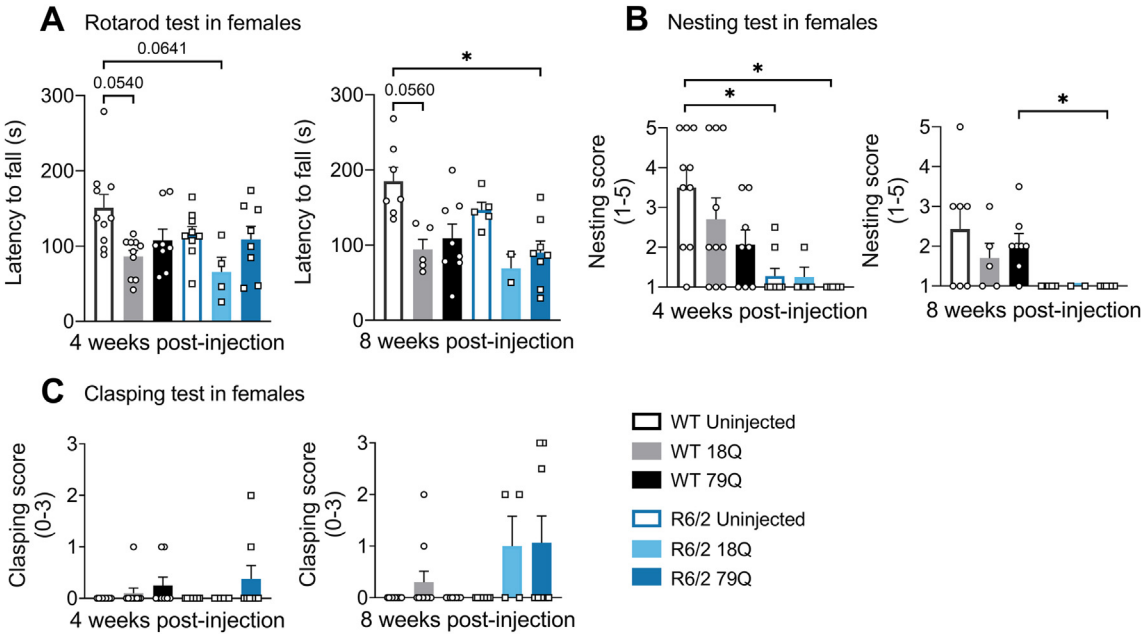

Figure 3: Behavioral analyses performed at 4- and 8 weeks post-injection in female R6/2 and WT after hypothalamic overexpression of 18Q and 79Q HTT. (A) In the rotarod test, R6/2 79Q showed a reduced latency to fall at 8 weeks post-injection (4 weeks n = 4–10/group, 8 weeks n = 2–8/group). (B) Reduced nest-building capacity in R6/2 mice (4 weeks n = 4–10/group, 8 weeks n = 2–8/group). (C) Overall no significant change was seen in the clasping phenotype (4 and 8 weeks n = 4–10/group). Data are expressed as mean ± SEM. Kruskal–Wallis tests followed by Dunn's *post hoc*. **Abbreviations:** WT = wild-type, 18Q = HTT853-18Q vector and 79Q = HTT853-79Q vector.

3.4. Weight changes after hypothalamic expression of 79Q HTT is accompanied by distinct transcriptional changes in gonadal white adipose tissue and hypothalamus

We then assessed whether gene expression changes in WAT are linked to increased adiposity in the gonadal visceral depot and differences in endpoint weight patterns in 79Q females. In gonadal WAT assessed at endpoint (11 weeks post-injection), both WT 79Q and R6/2 79Q had a significant reduction of beta-3 adrenergic receptor (B3AR) and adipose triglyceride lipase (ATGL) compared to uninjected groups (Figure 4A) with a significant vector effect (n = 8–11/group; 2-way ANOVA followed by Tukey's *post hoc*, $p < 0.0001$). R6/2 79Q further had a significant reduction in expression of peroxisome proliferator-activated receptor-gamma (PPARγ) compared to R6/2 uninjected. In contrast to gonadal WAT, no significant change in B3AR BAT mRNA was found in 79Q groups compared to uninjected groups of matching genotypes (Figure 4B). We next investigated BAT uncoupling protein 1 (UCP1) mRNA and found a significant effect of genotype (n = 9/group; 2-way ANOVA followed by Tukey's *post hoc*, $p = 0.0001$), where UCP1 was downregulated in the R6/2 uninjected vs. WT uninjected comparison and WT 79Q vs. R6/2 79Qs.

As WT- and R6/2 females with 79Q overexpression showed distinct metabolic phenotypes at 11 weeks post-injection (weight gain and weight loss respectively), with a shared feature of increased adiposity and downregulation of B3AR and ATGL, key mediators of lipolysis [45,46], we next established expression profiles of hypothalamic targets with suggested central roles in obesity and modulation of adipose tissue, including oxytocin [47,48], orexin [49,50], pro-opiomelanocortin (POMC) [51,52], brain-derived neurotrophic factor (BDNF) [53] and dopamine receptor D2 (DRD2) [54,55]. These markers are also known to be selectively altered in HD patients and mouse models [15,21,56]. At the endpoint of 11 weeks post-injection, mRNA levels of orexin, oxytocin and BDNF were significantly reduced in R6/2 79Q compared to WT uninjected (Figure 4C), and for the R6/2 79Q vs. WT 18Q comparison reduced POMC mRNA. WT 79Q displayed negative mean differences compared to WT uninjected (Orexin: −0.80, Oxytocin: −0.88, BDNF -0.64 and POMC -0.45). Expression of DRD2 remained unaffected in all groups. For 18Q groups, no significant impact on hypothalamic gene profile was seen compared to their uninjected group of matching genotypes.

4. DISCUSSION

Clinical HD is often associated with weight loss. Weight loss occurs despite adequate nutrition [5,57] and has in several cases been shown to begin already during premanifest disease [58,59]. Importantly, a higher BMI has been linked to slower disease progression [11]. Hypothalamic alterations were seen in HD patients [15,16] and several studies in mouse models have provided supportive evidence implicating mHTT-mediated pathology in the hypothalamus as a key contributor to metabolic dysfunction and other non-motor symptoms [17–19].

Gender differences may play a role in HD progression. Disease severity and rate of motor symptoms have been indicated to progress faster in women than men with HD [60–62]. Previous studies have shown that sex influences the progression of HD metabolic and behavioral phenotypes in various HD animal models [63–65]. Recently, we showed that hypothalamic mutant HTT expression led to a severe metabolic phenotype with obesity in only female mice [27]. As the degree of weight gain was pronounced in females, we focused on investigating factors related to weight gain in female R6/2 and BACHD mice.

In the present study, we found that overexpressing wtHTT (18Q) and mHTT (79Q) in the hypothalamus of female mice elicit different effects on metabolic phenotype in the R6/2 and BACHD mouse models and their respective WT littermates. In BACHD female mice associated with an obese phenotype, hypothalamic wtHTT (18Q) overexpression induces weight gain, although to a lesser extent as mHTT (79Q)

 © 2022 The Authors. Published by Elsevier GmbH. This is an open access article under the CC BY-NC-ND license (http://creativecommons.org/licenses/by-nc-nd/4.0/).

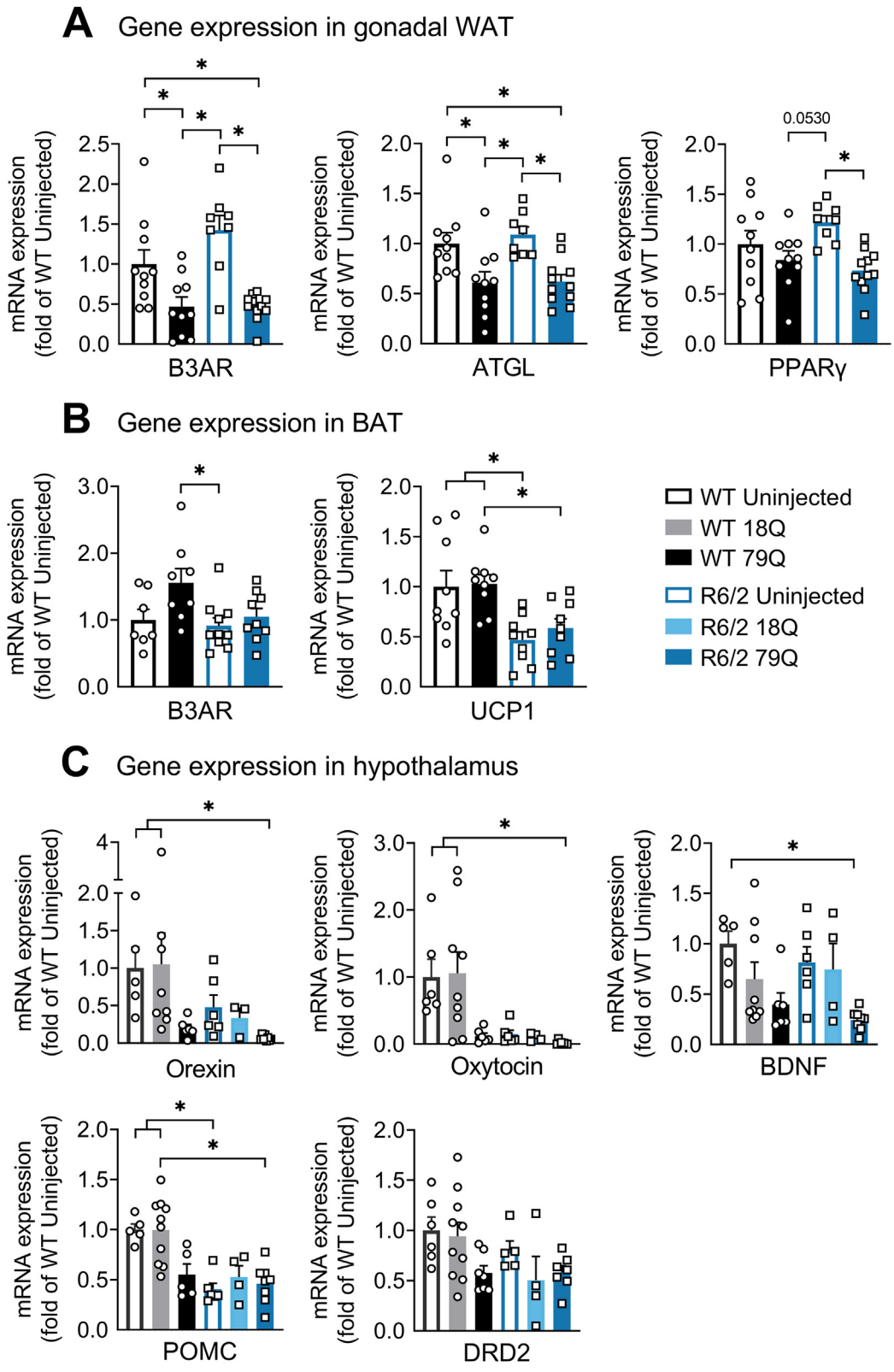

Figure 4: During late-stage weight loss in female R6/2 with hypothalamic 79Q HTT overexpression, significant mRNA changes are present in gonadal white adipose tissue and hypothalamus. Gene expression analysis was performed in gonadal WAT, BAT, and hypothalamus at the endpoint of 11-weeks post-injection. (A) 79Q groups showed distinct changes in B3AR, ATGL, and PPARγ, regulatory markers of adiposity and function in gonadal WAT (n = 8–11/group; 2-way ANOVA followed by Tukey's *post hoc*). (B) R6/2 BAT displayed a reduction in UCP1 levels (n = 9/group, 2-way ANOVA followed by Tukey's *post hoc*). (C) 18Q and 79Q overexpression caused distinct alterations in mRNA levels of hypothalamic markers in WT and R6/2 females (n = 3–10/group; Kruskal–Wallis test followed by Dunn's *post hoc*). Data are expressed as mean ± SEM. **Abbreviations:** WT = wild-type, 18Q = HTT853-18Q vector, 79Q = HTT853-79Q vector, WAT = white adipose tissue, BAT = brown adipose tissue.

 © 2022 The Authors. Published by Elsevier GmbH. This is an open access article under the CC BY-NC-ND license (http://creativecommons.org/licenses/by-nc-nd/4.0/).

overexpression. This indicates that normal HTT exerts an effect on body weight through hypothalamic pathways. In comparison, in the R6/2 model that is associated with a lean phenotype with end-stage weight loss, different effects on body weight in females were induced after expression of 18Q (no effect) or 79Q (significant early weight gain). However, weight gain in R6/2 79Q females was temporary and the disease progresses body weight loss was apparent. This indicates that the influence of the hypothalamus on body weight can, to some extent, be manipulated through overexpression of 79Q in an HD model that displays weight loss.

We further show that R6/2 79Q females display transcriptional downregulation in key genes involved in regulating adiposity and function. In contrast to untreated R6/2 analyzed during the same point in time, the WAT mRNA profile was comparable to WT females. In BAT, UCP1 levels were reduced in R6/2 groups and were not further modified by 79Q overexpression. Downregulation of UCP1 in BAT has previously been described in mouse models of HD [66] and WT mice overexpressing hypothalamic mHTT [18]. Distinct adipose tissue changes in 79Q mice were further associated with HTT-mediated changes in hypothalamic mRNA profile. The hypothalamus is tightly linked to peripheral tissue including the adipose tissue, while peripheral signals, in turn, act on the hypothalamus providing information on the energy status of the body [67,68]. Previous studies have highlighted that deficiency of hypothalamic neuropeptides causes obesity, including depletion of orexin [69], oxytocin [48], and POMC [70]. Moreover, there is an emerging role for hypothalamic BDNF signaling in body weight through the modulation of adiposity and BAT thermogenesis [71]. In the present study, BDNF expression levels were selectively reduced in R6/2 79Q females while R6/2 18Q and R6/2 uninjected were comparable to WT groups. Depletion of both anorectic and orexigenic neuropeptides and observations of higher food intake in WT 79Q and R6/2 79Q described here likely reflects the complex regulation of food intake. Considering our findings of the diverse metabolic phenotypes resulting from our strategy of hypothalamic overexpression of HTT fragments in the R6/2 model, future studies need to elaborate on how such rapid alterations in metabolic homeostasis and body weight affects a system that is already pathologically modified by the mutant CAG expansion in HTT.

In all R6/2 groups, regardless of body weight and food intake patterns, there was an onset of characteristic weight loss during mid/late-stage timepoints. This further highlights pathological alterations of the metabolic system in R6/2 mice over time. The effect of mHTT is likely to occur in tissues and organs all through the body [12,72]. Other strategies of targeting energy metabolism to slow disease progression, such as inducing leptin deficiency through a genetic crossing of the R6/2 model, have also been found insufficient to modify end-stage weight loss [65]. Cell-intrinsic effects of mHTT in peripheral tissue could explain this. Among characteristic hallmarks are severe skeletal muscle wasting [73], abdominal fat changes [20] as well as hyperglycemia and hypoinsulinemia in the late stages [74]. Notably, in *vivo* transgenic *Drosophila* models of HD with neuronal expression of exon 1 of a human mHTT (93Q) fragment display progressive decline in body weight that is predominately associated with declining total lipid levels and accompanied with alterations in abdominal fat body lipid droplet size throughout the disease [75]. Similar to R6/2, clinical HD is associated with widespread peripheral pathology, including adipose tissue alterations [11,76] and a higher BMI has been shown to be linked to a slower disease progression, indicating several possibilities for therapeutic intervention that may also prove beneficial for the amelioration of central pathology [77].

Even though this study focused on exploring disease features in females, we in addition analyzed a smaller group of male mice in both models using the same experimental setup. Hence, deterioration in motor performance of the R6/2 79Q group underlines the need of further analysis of phenotype with additional behavior tests and a larger group of animals.

5. CONCLUSIONS

Collectively, we provide further support for the role of HTT (both wt and mutant) in metabolic control via hypothalamic neurocircuits. More studies are needed to further delineate the effect of altered HTT function in hypothalamic populations and to understand how disrupted central- and peripheral crosstalks impact HD pathogenesis. Collectively, this may provide further strategies and targets for therapeutic intervention.

SOURCE OF FUNDING

This study was financially supported by the Swedish Research Council (grant number 2017/01080). Å.P. was supported by the Swedish Research Council (grant number 2018/02559), the Province of Skåne State Grants (ALF) as well as the Knut and Alice Wallenberg Foundation (grant number 2019.0467). R.S.K. was supported by the Swedish Society for Medical Research fellowship.

AUTHOR CONTRIBUTIONS

M.B., Å.P., R.S.K., and E.D. conceived and designed the experiments. E.D. and R.S.K. performed the experiments and analyzed the data. E.D. and M.B. wrote the first draft of the manuscript. All authors reviewed the manuscript and approved the final version.

ACKNOWLEDGMENTS

We thank Björn Anzelius, Anna S Hansen, Anneli Josefsson, Susanne Jonsson, Ann-Charlotte Selberg, Catarina Blennow and Ulla Samuelsson at Lund University for excellent technical assistance. The authors would also like to thank Helene Jacobsson at Lund University for consultation regarding statistics and performing the time-course body weight analyses.

CONFLICT OF INTEREST

None declared.

APPENDIX A. SUPPLEMENTARY DATA

Supplementary data to this article can be found online at https://doi.org/10.1016/j.molmet.2022.101439.

REFERENCES

[1] Vonsattel, J.P., Keller, C., Cortes Ramirez, E.P., 2011. Huntington's disease - neuropathology. Handbook of Clinical Neurology 100:83—100.

[2] Vonsattel, J.P., Myers, R.H., Stevens, T.J., Ferrante, R.J., Bird, E.D., Richardson, Jr., E.P., 1985. Neuropathological classification of Huntington's disease. Journal of Neuropathology & Experimental Neurology 44(6):559—577.

[3] Goodman, A.O., Murgatroyd, P.R., Medina-Gomez, G., Wood, N.I., Finer, N., Vidal-Puig, A.J., et al., 2008. The metabolic profile of early Huntington's disease—a combined human and transgenic mouse study. Experimental Neurology 210(2):691—698.

 © 2022 The Authors. Published by Elsevier GmbH. This is an open access article under the CC BY-NC-ND license (http://creativecommons.org/licenses/by-nc-nd/4.0/).

[4] Djoussé, L., Knowlton, B., Cupples, L.A., Marder, K., Shoulson, I., Myers, R.H., 2002. Weight loss in early stage of Huntington's Disease. Neurology 59(9): 1325–1330.

[5] Sanberg, P.R., Fibiger, H.C., Mark, R.F., 1981. Body weight and dietary factors in Huntington's disease patients compared with matched controls. Medical Journal of Australia 1(8):407–409.

[6] Valenza, M., Rigamonti, D., Goffredo, D., Zuccato, C., Fenu, S., Jamot, L., et al., 2005. Dysfunction of the cholesterol biosynthetic pathway in Huntington's disease. Journal of Neuroscience 25(43):9932–9939.

[7] Block, R.C., Dorsey, E.R., Beck, C.A., Brenna, J.T., Shoulson, I., 2010. Altered cholesterol and fatty acid metabolism in Huntington disease. Journal of Clinical Lipidology 4(1):17–23.

[8] Farrer, L.A., 1985. Diabetes mellitus in Huntington disease. Clinical Genetics 27(1):62–67.

[9] Podolsky, S., Leopold, N., Sax, D., 1972. Increased frequency of diabetes mellitus in patients with Huntington's chorea. The Lancet 299(7765):1356–1359.

[10] Lalić, N.M., Marić, J., Svetel, M., Jotić, A., Stefanova, E., Lalić, K., et al., 2008. Glucose homeostasis in Huntington disease: abnormalities in insulin sensitivity and early-phase insulin secretion. Archives of Neurology 65(4):476–480.

[11] van der Burg, J.M.M., Gardiner, S.L., Ludolph, A.C., Landwehrmeyer, G.B, Roos, R.A.C., Aziz, N.A., 2017. Body weight is a robust predictor of clinical progression in Huntington disease. Annals of Neurology 82(3):479–483.

[12] van der Burg, J.M.M., Björkqvist, M., Brundin, P., 2009. Beyond the brain: widespread pathology in Huntington's disease. The Lancet Neurology 8(8):765–774.

[13] Aziz, N.A., Roos, R.A.C., 2013. Characteristics, pathophysiology and clinical management of weight loss in Huntington's disease. Neurodegenerative Disease Management 3(3):253–266.

[14] Saper, C.B., Lowell, B.B., 2014. The hypothalamus. Current Biology 24(23): R1111–R1116.

[15] Gabery, S., Murphy, K., Schultz, K., Loy, C.T., McCusker, E., Kirik, D., et al., 2010. Changes in key hypothalamic neuropeptide populations in Huntington disease revealed by neuropathological analyses. Acta Neuropathologica 120(6):777–788.

[16] Soneson, C., Fontes, M., Zhou, Y., Denisov, V., Paulsen, J.S., Kirik, D., et al., 2010. Early changes in the hypothalamic region in prodromal Huntington disease revealed by MRI analysis. Neurobiology of Disease 40(3):531–543.

[17] Hult, S., Soylu, R., Björklund, T., Belgardt, B.F., Mauer, J., Brüning, J.C., et al., 2011. Mutant huntingtin causes metabolic imbalance by disruption of hypothalamic neurocircuits. Cell Metabolism 13(4):428–439.

[18] Soylu-Kucharz, R., Adlesic, N., Baldo, B., Kirik, D., Petersén, Å., 2015. Hypothalamic overexpression of mutant huntingtin causes dysregulation of brown adipose tissue. Scientific Reports 5(1):14598.

[19] Hult Lundh, S., Nilsson, N., Soylu, R., Kirik, D., Petersén, Å., 2013. Hypothalamic expression of mutant huntingtin contributes to the development of depressive-like behavior in the BAC transgenic mouse model of Huntington's disease. Human Molecular Genetics 22(17):3485–3497.

[20] Björkqvist, M., Petersén, Å., Bacos, K., Isaacs, J., Norlén, P., Gil, J., et al., 2006. Progressive alterations in the hypothalamic-pituitary-adrenal axis in the R6/2 transgenic mouse model of Huntington's disease. Human Molecular Genetics 15(10):1713–1721.

[21] Petersén, Å., Gil, J., Maat-Schieman, M.L.C., Björkqvist, M., Tanila, H., Araújo, I.M., et al., 2004. Orexin loss in Huntington's disease. Human Molecular Genetics 14(1):39–47.

[22] Papalexi, E., Persson, A., Björkqvist, M., Petersén, Å., Woodman, B., Bates, G.P., et al., 2005. Reduction of GnRH and infertility in the R6/2 mouse model of Huntington's disease. European Journal of Neuroscience 22(6): 1541–1546.

[23] Mangiarini, L., Sathasivam, K., Seller, M., Cozens, B., Harper, A., Hetherington, C., et al., 1996. Exon 1 of the HD gene with an expanded CAG repeat is sufficient to cause a progressive neurological phenotype in transgenic mice. Cell 87(3):493–506.

[24] van der Burg, J.M.M., Bacos, K., Wood, N.I., Lindqvist, A., Wierup, N., Woodman, B., et al., 2008. Increased metabolism in the R6/2 mouse model of Huntington's disease. Neurobiology of Disease 29(1):41–51.

[25] Cattaneo, E., Zuccato, C., Tartari, M., 2005. Normal huntingtin function: an alternative approach to Huntington's disease. Nature Reviews Neuroscience 6(12):919–930.

[26] Van Raamsdonk, J.M., Gibson, W.T., Pearson, J., Murphy, Z., Lu, G., Leavitt, B.R., et al., 2006. Body weight is modulated by levels of full-length Huntingtin. Human Molecular Genetics 15(9):1513–1523.

[27] Soylu-Kucharz, R., Khoshnan, A., Petersén, Å., 2022. IKKβ signaling mediates metabolic changes in the hypothalamus of a Huntington's disease mouse model. iScience. https://doi.org/10.1016/j.isci.2022.103771.

[28] Gray, M., Shirasaki, D.I., Cepeda, C., André, V.M., Wilburn, B., Lu, X., et al., 2008. Full-length human mutant huntingtin with a stable polyglutamine repeat can elicit progressive and selective neuropathogenesis in BACHD mice. Journal of Neuroscience : The Official Journal of the Society for Neuroscience 28(24): 6182–6195.

[29] Carter, R.J., Lione, L.A., Humby, T., Mangiarini, L., Mahal, A., Bates, G.P., et al., 1999. Characterization of progressive motor deficits in mice transgenic for the human Huntington's disease mutation. Journal of Neuroscience 19(8): 3248–3257.

[30] Morton, A.J., Glynn, D., Leavens, W., Zheng, Z., Faull, R.L.M., Skepper, J.N., et al., 2009. Paradoxical delay in the onset of disease caused by super-long CAG repeat expansions in R6/2 mice. Neurobiology of Disease 33(3):331–341.

[31] Soylu-Kucharz, R., Sandelius, Å., Sjögren, M., Blennow, K., Wild, E.J., Zetterberg, H., et al., 2017. Neurofilament light protein in CSF and blood is associated with neurodegeneration and disease severity in Huntington's disease R6/2 mice. Scientific Reports 7(1):14114.

[32] Deacon, R.M.J., 2006. Assessing nest building in mice. Nature Protocols 1(3): 1117–1119.

[33] Lalonde, R., Strazielle, C., 2011. Brain regions and genes affecting limb-clasping responses. Brain Research Reviews 67(1–2):252–259.

[34] Guyenet, S.J., Furrer, S.A., Damian, V.M., Baughan, T.D., La Spada, A.R., Garden, G.A., 2010. A simple composite phenotype scoring system for evaluating mouse models of cerebellar ataxia. Journal of Visualized Experiments(39).

[35] Livak, K.J., Schmittgen, T.D., 2001. Analysis of relative gene expression data using real-time quantitative PCR and the 2(-Delta Delta C(T)) Method. Methods 25(4):402–408.

[36] DiFiglia, M., Sapp, E., Chase, K.O., Davies, S.W., Bates, G.P., Vonsattel, J.P., et al., 1997. Aggregation of huntingtin in neuronal intranuclear inclusions and dystrophic neurites in brain. Science 277(5334):1990–1993.

[37] Vonsattel, J.P., DiFiglia, M., 1998. Huntington disease. Journal of Neuropathology & Experimental Neurology 57(5):369–384.

[38] Davies, S.W., Turmaine, M., Cozens, B.A., DiFiglia, M., Sharp, A.H., Ross, C.A., et al., 1997. Formation of neuronal intranuclear inclusions underlies the neurological dysfunction in mice transgenic for the HD mutation. Cell 90(3):537–548.

[39] Meade, C.A., Deng, Y.P., Fusco, F.R., Del Mar, N., Hersch, S., Goldowitz, D., et al., 2002. Cellular localization and development of neuronal intranuclear inclusions in striatal and cortical neurons in R6/2 transgenic mice. Journal of Comparative Neurology 449(3):241–269.

[40] Sun, M., Choi, E.Y., Magee, D.J., Stets, C.W., During, M.J., Lin, E.D., 2014. Metabolic effects of social isolation in adult C57BL/6 mice. International Scholarly Research Notices 2014:690950.

[41] Kalliokoski, O., Jacobsen, K.R., Darusman, H.S., Henriksen, T., Weimann, A., Poulsen, H.E., et al., 2013. Mice do not habituate to metabolism cage housing–a three week study of male BALB/c mice. PLoS One 8(3):e58460.

 © 2022 The Authors. Published by Elsevier GmbH. This is an open access article under the CC BY-NC-ND license (http://creativecommons.org/licenses/by-nc-nd/4.0/).

[42] Neely, C.L.C., Pedemonte, K.A., Boggs, K.N., Flinn, J.M., 2019. Nest building behavior as an early indicator of behavioral deficits in mice. Journal of Visualized Experiments 152.
[43] Jirkof, P., 2014. Burrowing and nest building behavior as indicators of well-being in mice. Journal of Neuroscience Methods 234:139–146.
[44] Sjögren, M., Duarte, A.I., McCourt, A.C., Shcherbina, L., Wierup, N., Björkqvist, M., 2017. Ghrelin rescues skeletal muscle catabolic profile in the R6/2 mouse model of Huntington's disease. Scientific Reports 7(1):13896.
[45] Young, S.G., Zechner, R., 2013. Biochemistry and pathophysiology of intravascular and intracellular lipolysis. Genes & Development 27(5):459–484.
[46] Lafontan, M., Berlan, M., 1993. Fat cell adrenergic receptors and the control of white and brown fat cell function. Journal of Lipid Research 34(7):1057–1091.
[47] Yuan, J., Zhang, R., Wu, R., Gu, Y., Lu, Y., 2020. The effects of oxytocin to rectify metabolic dysfunction in obese mice are associated with increased thermogenesis. Molecular and Cellular Endocrinology 514:110903.
[48] Ding, C., Leow, M.K., Magkos, F., 2019. Oxytocin in metabolic homeostasis: implications for obesity and diabetes management. Obesity Reviews 20(1): 22–40.
[49] Perez-Leighton, C.E., Billington, C.J., Kotz, C.M., 2014. Orexin modulation of adipose tissue. Biochimica et Biophysica Acta - Molecular Basis of Disease 1842(3):440–445.
[50] Butterick, T.A., Billington, C.J., Kotz, C.M., Nixon, J.P., 2013. Orexin: pathways to obesity resistance? Reviews in Endocrine & Metabolic Disorders 14(4):357–364.
[51] Shin, A.C., Filatova, N., Lindtner, C., Chi, T., Degann, S., Oberlin, D., et al., 2017. Insulin receptor signaling in POMC, but not AgRP, neurons controls adipose tissue insulin action. Diabetes 66(6):1560–1571.
[52] Lindberg, I., Fricker, L.D., 2021. Obesity, POMC, and POMC-processing enzymes: surprising results from animal models. Endocrinology 162(12):bqab155.
[53] Wang, P., Loh, K.H., Wu, M., Morgan, D.A., Schneeberger, M., Yu, X., et al., 2020. A leptin–BDNF pathway regulating sympathetic innervation of adipose tissue. Nature 583(7818):839–844.
[54] Wang, X., Villar, V.A., Tiu, A., Upadhyay, K.K, Cuevas, S., 2018. Dopamine D2 receptor upregulates leptin and IL-6 in adipocytes. The Journal of Lipid Research 59(4):607–614.
[55] Tavares, G., Martins, F.O., Melo, B.F., Matafome, P., Conde, S.V., 2011. Peripheral dopamine directly acts on insulin-sensitive tissues to regulate insulin signaling and metabolic function. Frontiers in Pharmacology 2021:12.
[56] Baldo, B., Gabery, S., Soylu-Kucharz, R., Cheong, R.Y., Henningsen, J.B., Englund, E., et al., 2019. SIRT1 is increased in affected brain regions and hypothalamic metabolic pathways are altered in Huntington disease. Neuropathology and Applied Neurobiology 45(4):361–379.
[57] Trejo, A., Tarrats, R.M., Alonso, M.E., Boll, M., Ochoa, A., Velásquez, L., 2004. Assessment of the nutrition status of patients with Huntington's disease. Nutrition 20(2):192–196.
[58] Khan, W., Alusi, S., Tawfik, H., Hussain, A., 2021. The relationship between non-motor features and weight-loss in the premanifest stage of Huntington's disease. PLoS One 16(7):e0253817.
[59] Mochel, F., Charles, P., Seguin, F., Barritault, J., Coussieu, C., Perin, L., et al., 2007. Early energy deficit in Huntington disease: identification of a plasma biomarker traceable during disease progression. PLoS One 2(7):e647.
[60] Zielonka, D., Marinus, J., Roos, R.A.C., De Michele, G., Di Donato, S., Putter, H., et al., 2013. The influence of gender on phenotype and disease progression in patients with Huntington's disease. Parkinsonism & Related Disorders 19(2):192–197.
[61] Zielonka, D., Ren, R., De Michele, G., Roos, R.A.C., Squitieri, F., Bentivoglio, A.R., et al., 2018. The contribution of gender differences in motor, behavioral and cognitive features to functional capacity, independence and quality of life in patients with Huntington's disease. Parkinsonism & Related Disorders 49:42–47.
[62] Zielonka, D., Stawinska-Witoszynska, B., 2020. Gender differences in non-sex linked disorders: insights from Huntington's disease. Frontiers in Neurology 11:571.
[63] Dorner, J.L., Miller, B.R., Barton, S.J., Brock, T.J., Rebec, G.V., 2007. Sex differences in behavior and striatal ascorbate release in the 140 CAG knock-in mouse model of Huntington's disease. Behavioural Brain Research 178(1):90–97.
[64] Soylu-Kucharz, R., Baldo, B., Petersen, A., 2016. Metabolic and behavioral effects of mutant huntingtin deletion in Sim1 neurons in the BACHD mouse model of Huntington's disease. Scientific Reports 6:28322.
[65] Sjögren, M., Soylu-Kucharz, R., Dandunna, U., Stan, T.L, Cavalera, M., Sandelius, Å., et al., 2019. Leptin deficiency reverses high metabolic state and weight loss without affecting central pathology in the R6/2 mouse model of Huntington's disease. Neurobiology of Disease 132:104560.
[66] Lindenberg, K.S., Weydt, P., Müller, H.P., Bornstedt, A., Ludolph, A.C., Landwehrmeyer, G.B., et al., 2014. Two-point magnitude MRI for rapid mapping of brown adipose tissue and its application to the R6/2 mouse model of Huntington disease. PLoS One 9(8):e105556.
[67] Timper, K., Brüning, J.C., 2017. Hypothalamic circuits regulating appetite and energy homeostasis: pathways to obesity. Disease Models & Mechanisms 10(6):679–689.
[68] Contreras, C., Nogueiras, R., Diéguez, C., Rahmouni, K., López, M., 2017. Traveling from the hypothalamus to the adipose tissue: the thermogenic pathway. Redox Biology 12:854–863.
[69] Hara, J., Beuckmann, C.T., Nambu, T., Willie, J.T., Chemelli, R.M., Sinton, C.M., et al., 2001. Genetic ablation of orexin neurons in mice results in narcolepsy, hypophagia, and obesity. Neuron 30(2):345–354.
[70] Yaswen, L., Diehl, N., Brennan, M.B., Hochgeschwender, U., 1999. Obesity in the mouse model of pro-opiomelanocortin deficiency responds to peripheral melanocortin. Nature Medicine 5(9):1066–1070.
[71] Cao, L., Choi, E.Y., Liu, X., Martin, A., Wang, C., Xu, X., et al., 2011. White to Brown fat phenotypic switch induced by genetic and environmental activation of a hypothalamic-adipocyte Axis. Cell Metabolism 14(3):324–338.
[72] Sathasivam, K., Hobbs, C., Turmaine, M., Mangiarini, L., Mahal, A., Bertaux, F., et al., 1999. Formation of polyglutamine inclusions in non-CNS tissue. Human Molecular Genetics 8(5):813–822.
[73] She, P., Zhang, Z., Marchionini, D., Diaz, W.C., Jetton, T.J., Kimball, S.R., et al., 2011. Molecular characterization of skeletal muscle atrophy in the R6/2 mouse model of Huntington's disease. American Journal of Physiology. Endocrinology and Metabolism 301(1):E49–E61.
[74] Björkqvist, M., Fex, M., Renström, E., Wierup, N., Petersén, Å., Gil, J., et al., 2005. The R6/2 transgenic mouse model of Huntington's disease develops diabetes due to deficient beta-cell mass and exocytosis. Human Molecular Genetics 14(5):565–574.
[75] Aditi, K., Shakarad, M.N., Agrawal, N., 2016. Altered lipid metabolism in Drosophila model of Huntington's disease. Scientific Reports 6(1):31411.
[76] McCourt, A.C., Parker, J., Silajdžić, E., Haider, S., Sethi, H., Tabrizi, S.J., et al., 2015. Analysis of white adipose tissue gene expression reveals CREB1 pathway altered in Huntington's disease. Journal of Huntington's Disease 4:371–382.
[77] Carroll, J.B., Bates, G.P, Steffan, J., Saft, C., Tabrizi, S.J., 2015. Treating the whole body in Huntington's disease. The Lancet Neurology 14(11):1135–1142.

 © 2022 The Authors. Published by Elsevier GmbH. This is an open access article under the CC BY-NC-ND license (http://creativecommons.org/licenses/by-nc-nd/4.0/).